Graphene-Alginate Fluids as Unconventional Electrodes for the Electrokinetic Remediation of Cr(VI)

Alicia Telepanich · Tatianna Marshall ·
Stefano Gregori · Alejandro G. Marangoni ·
Erica Pensini

Abstract Electrokinetic remediation of groundwater pollutants uses electrical fields to draw contaminants towards electrodes, where they are removed through diverse mechanisms. Conventional electrodes are installed in discrete positions in the soil. Here, we develop unconventional electrodes for the electrokinetic remediation of Cr(VI). Our electrodes are fluids comprised of sodium alginate and graphene particles in aqueous solution and can therefore be injected in the location of interest to facilitate their installation. The subsequent injection of $CaCl_2$ solutions induces gelation (as demonstrated by shear rheology), forming a conductive material (as demonstrated by voltammetry experiments). This material sorbed Cr(VI), as demonstrated in sorption experiments conducted under no-flow conditions and even without any applied electric potential. Therefore, it could be placed downstream of the pollutant to act as a barrier, controlling Cr(VI) migration and providing protection for human or ecological receptors. In a saturated model sandy aquifer, Cr(VI) was drawn towards our unconventional electrode barrier using a 12 V differential voltage, thereby decreasing its concentrations by approximately 70% in 30 min (starting from 0.35 mM Cr(VI), as demonstrated using a spectrophotometer). The net reduction of Cr(VI) concentrations in water was achieved without its extraction from the electrode proximity, because our graphene-alginate electrodes sorbed Cr(VI). Our findings provide a proof of concept of a novel remediation approach, which combines electrokinetic remediation with injectable barriers.

Keywords Electrokinetic remediation · Gels · Graphene · Voltammetry · Rheology

A. Telepanich · T. Marshall · S. Gregori · E. Pensini (✉)
School of Engineering, University of Guelph, Room 2525 Richards Bld., 50 Stone Road East, ON N1G 2W1 Guelph, Canada
e-mail: epensini@uoguelph.ca

A. G. Marangoni
Food Science Department, University of Guelph, 50 Stone Road East, Guelph, ON N1G 2W1, Canada

1 Introduction

Cr(VI) is a highly toxic compound, which causes nausea, diarrhea, liver and kidney damage, dermatitis, internal hemorrhage, and respiratory problems (Iyer et al., 2019; Pensini et al., 2018; Siwik et al., 2019). The maximum allowable concentrations of Cr(VI) in groundwater are recommended by environmental agencies. For instance, in the USA, the Environmental Protection Agency (EPA) recommends maximum concentrations of total chromium of 100 µg/L in drinking water. Despite regulatory limits, a significant number of sites are polluted by Cr(VI), due to

its wide use in industry (e.g., alloy production and plating, wood preservation, and leather tanning) (Němeček et al., 2015).

While Cr(VI) is highly toxic and mobile, its trivalent counterpart (Cr(III)) is scarcely mobile in aquifers and less toxic (Dinesh & Pittman, 2006; Pensini et al., 2018). The risk associated with heavy metals in groundwater typically decreases with decreasing mobility (Huang et al., 2017; Pensini et al., 2018; Siwik et al., 2019). Also, in trace amounts, Cr(III) is an essential element in the metabolism of mammals, because it reduces blood glucose and cholesterol levels, in addition to aiding in muscle development (Pensini et al., 2018). Therefore, the reduction of Cr(VI) to Cr(III) has been the objective of diverse approaches for the remediation of aquifers polluted by Cr(VI).

In situ remediation methods used to reduce Cr(VI) to Cr(III) include biological (biotic) and chemical (abiotic) approaches. The biotic reduction of Cr(VI) can be achieved in the presence of suitable bacterial populations (Němeček et al., 2015, 2016; Thatoi et al., 2014). The abiotic reduction of Cr(VI) can be achieved using nanoscale zero-valent iron (nZVI) or nZVI stabilized by biochar (Němeček et al., 2015; Su et al., 2016), ferrous sulfate (Palma et al., 2015), or other forms of iron (Karn et al., 2009). The use of nZVI has shown success in a number of polluted sites, but particle reactivity decreases over time, and there are concerns regarding the potential toxicity of nanoparticles (Guan et al., 2015). These remediation methods would not prevent Cr(VI) immobilization during treatment, and Cr(VI) is highly mobile (thereby posing risks to downstream receptors).

Barriers can be utilized to prevent contaminant migration. The installation of barriers that require soil excavation may be challenging and costly, but injectable barriers allow avoiding soil excavation, as we described in our previous manuscripts (Estepa et al., 2020; Marshall et al., 2020a, 2020b). In the case of Cr(VI), our previous studies proposed simultaneously trapping and treating Cr(VI) (Pensini et al., 2018; Siwik et al., 2019). This objective was achieved with injectable fluids, obtained with environmentally friendly polymers, such as scleroglucan and guar, and containing the reducing agent sodium thiosulfate (Pensini et al., 2018; Siwik et al., 2019). These fluids had low viscoelasticity before contact with Cr(VI), enabling their injection, and gelled on

demand in Cr(VI) proximity, to trap the pollutant while reducing it to Cr(III). Our previous studies were conducted using high Cr(VI) concentrations (Pensini et al., 2018; Siwik et al., 2019). Our previously proposed remediation required a minimum Cr(VI) concentration to ensure Cr(VI) trapping, because chromium acted as crosslinker (as a general rule, below benchmark concentrations, crosslinkers do not enable gelation).

In some instances, contaminated soil can be excavated and treated ex situ, using either mechanical separation or pyrometallurgical separation (Huang et al., 2017). However, as discussed above, soil excavation is challenging for deep contamination.

Other methods proposed for the remediation of heavy metals include phytoremediation (which relies on the plant root system to extract shallow contaminants), pump and treat, and soil flushing (Huang et al., 2017; Marshall et al., 2020c). Pump and treat involves pumping of polluted groundwater, ex situ treatment, and finally its reinjection into the aquifer (Marshall et al., 2020c). Soil flushing involves that use of additives which enhance contaminant solubilization and their extraction, e.g., through pump and treat (Huang et al., 2017).

Electrokinetic remediation has also been proposed to treat Cr(VI) (Huang et al., 2017; Mulligan et al., 2001; Sawada et al., 2004), and it also been successfully used to remove other ionic forms of contaminants (Virkutyte et al., 2002). Electrokinetic remediation involves the use of electrodes, towards which contaminants are transported due to electromigration, electrophoresis, electroosmosis (in the case of non-charged contaminants), and diffusion (Virkutyte et al., 2002). Here, contaminants are removed through electroplating of metal electrodes, adsorption onto the electrode, precipitation or co-precipitation at the electrode, pumping in the electrode proximity, complexing with ion-exchange resins (Lu et al., 2012), or sorption onto materials such as activated carbon (Sawada et al., 2004). Electrokinetic remediation offers the advantage of being suitable for a wide range of soils, including soils with scarce permeability (Reddy et al., 2009). Also, while the present study focuses on Cr(VI), electrokinetic remediation can be applied to sites with mixed contaminants (e.g., organic compounds and heavy metals) (Coupled phenomena in environmental geotechnics xxxx). Different types of electrodes have been proposed for

electrokinetic remediation, including metal electrodes (e.g., stainless steel electrodes) (Kim et al., 2014), iron-loaded activated carbon electrodes (Yan et al., 2018), iridium-coated titanium (Kim et al., 2020), and polyaniline (PANI) immobilized on a support material to produce electrodes, because its amine functional groups could interact with anions (Wang et al., 2019). In a recent study, electrokinetic remediation was coupled with permeable reactive barriers for the treatment of aquifers polluted with cadmium (Zhou et al., 2020). These barriers required soil excavation to be installed.

In this study, we propose for the first time the use of injectable electrodes, which can also act as barriers. Our electrodes are produced using solutions of sodium alginate and conductive graphene nanoparticles, which can be injected in the desired location and subsequently gelled using $CaCl_2$ salt solutions. While graphene was previously used to increase the conductivity of polymeric materials (for instance, polyurethane (Pokharel et al., 2019)), it was not used before to produce injectable electrodes in the context of electrokinetic remediation. Sodium alginate was previously used to prepare switchable water in oil in water emulsions, which gelled on demand in hydrocarbon proximity or in contact with selected triggers (Lamont et al., 2019a, 2019b). Gelation was due to emulsion reversal, which caused mixing between $CaCl_2$ in the primary emulsion and the outer sodium alginate solution (Lamont et al., 2019a, 2019b). Upon gelation, sodium alginate–based fluids could trap hydrocarbons, but they were not electrically conductive (Lamont et al., 2019a, 2019b). Also, in another study, we incorporated carbon nanoparticles in zein-based injectable barriers, with the goal of reinforcing them and rendering them more impermeable (Marshall et al., 2020d), and in hydroxyethylcellulose fluids to enhance their viscosity (hence temporarily confining contaminants) (Marshall et al., 2020a). However, the carbon nanoparticles used in our previous studies were not conductive. Here, the scope of our research is to use sodium alginate crosslinked with $CaCl_2$ and containing graphene nanoparticles as a barrier and a cathode, to draw Cr(VI), sorb it and reduce it. Our injectable electrodes could prevent Cr(VI) downstream migration during its remediation. Previous studies used different electrolytes to increase conductivity (Reddy & Chinthamreddy, 2004). Here,

we propose to inject $CaCl_2$ in the polluted aquifer, to act both as crosslinker and electrolyte, thereby promoting electrokinetic flow.

2 Materials and Methods

2.1 Materials

Graphene nanoplatelets were purchased from Fisher Scientific (NP1, graphene nanoplatelets aggregates, sub-micron particles, surface are 500 m^2/g, Alfa Aesar) and from Sigma-Aldrich (NP2, graphene nanoplatelets, surface area 500 m^2/g, GNP-s, xGnP). Sodium alginate (alginic acid, sodium salt, Acros Organics), hexavalent chromium salt ($K_2Cr_2O_7$), and calcium chloride anhydrous (Dessicant ACS, EMD Millipore) were purchased from Fisher Scientific. Ottawa sand (W + I, BDH9274) was purchased from VWR (Canada). Aluminum electrodes (size = 9.8 cm × 1.8 cm × 1 mm) were purchased from a local metal shop. Deionized (DI) water was used in all experiments.

2.2 Electrokinetic Experiments

Electrokinetic experiments were conducted using a model sandy aquifer. This aquifer was created using Ottawa sand (39 g) and a rectangular cell (width = 2 cm, height = 6 cm, length = 5 cm), filled with 8.8 mL of DI water. After filling the cell with DI water, electrodes were injected. Liquid electrodes were prepared with 100 g/L or 200 g/L of either NP1 or NP2, premixed with 1 wt% sodium alginate solution in DI water. During the injection of the liquid electrodes, an equivalent volume of DI water was simultaneously extracted from the cell, to simulate groundwater displacement in a real aquifer. Subsequently, 500 µL of $CaCl_2$ solution (3 M) were injected in the same location where the alginate-graphene mixture was injected, inducing crosslinking (i.e., electrode gelation). Finally, the electrolyte (1.2 mL of 3 M $CaCl_2$ solution) and Cr(VI) (1.2 mL of 0.35 mM Cr(VI) solution) were injected and thoroughly mixed with the sand, to achieve homogenous Cr(VI) concentrations in the model aquifer. A water sample (1.2 mL) was then extracted, to determine with accuracy the initial Cr(VI) concentrations using

a spectrophotometer (SPECTRONIC™ 200 Spectro-photometer, Fisher Scientific, Canada) at a 352 nm wavelength and a calibration curve. An aluminum electrode (9.8 cm × 1.8 cm × 1 mm) was then installed at 2.5 cm distance from the alginate-graphene electrode. The two electrodes were then connected to a power source (Power Design Inc., 3650-S), and a differential voltage of 12 V was applied for 10 min, 15 min, and 30 min, using the alginate-graphene electrode as the cathode and the aluminum electrode as the anode. The setup used is shown in Fig. 1. At the end of electrokinetic experiments, water samples were collected again, from the entire cell area. The Cr(VI) concentration in the water was once again determined using a spectrophotometer (as described above), to estimate Cr(VI) removal efficiency. Experiments were conducted in triplicate.

2.3 Scanning Electron Microscopy (SEM)

SEM images of NP1 and NP2 were collected using a FEI Quanta FEG 250 SEM (Thermo Fisher
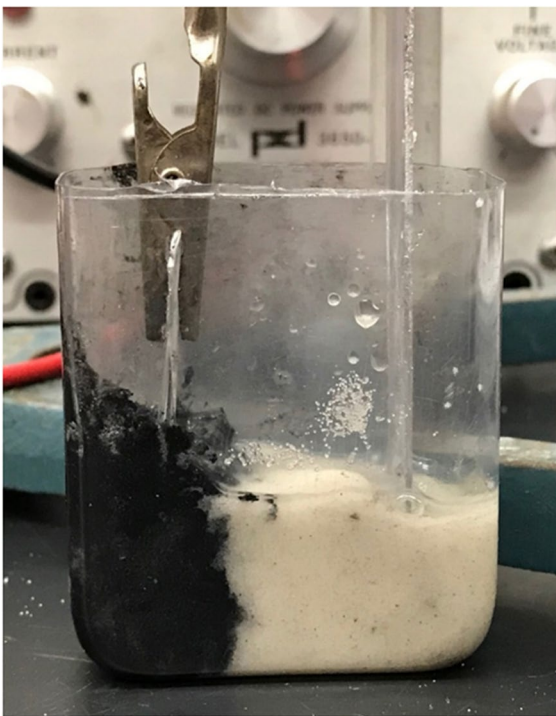

Fig. 1 Setup used to conduct electrokinetic separation experiments. The alginate-graphene cathode is on the left, and the aluminum electrode is on the right

Scientific), applying an accelerating voltage of 20 kV and a working distance of approximately 11 mm.

2.4 Cyclic Voltammetry Experiments

Cyclic voltammetry experiments were conducted to assess the electrical behavior of our electrodes, prepared using 1 wt% sodium alginate (5 mL), mixed with either 100 g/L or 200 g/L NP1 or NP2, and subsequently crosslinked with 3 M CaCl$_2$ (500 μL). Samples without either NP1 or NP2 were also analyzed for comparison. The size of the alginate electrode material was approximately 2.5 cm × 1.5 cm. This material was connected to a source measure unit (Keithley 2602) using conductive wires and alligator clips and exposed to a cyclical voltage varied either between − 0.5 and + 0.5 V (with steps of 50 mV, a 2-s delay between steps, and a total of 10 cycles) or between − 5 and + 5 V (with steps of 0.5 V, a 2-s delay between steps, and a total of 5 cycles).

2.5 Shear Rheology Experiments (Strain Amplitude Sweeps)

Shear rheology experiments were conducted with a torque-controlled rheometer (MCR302 Anton Paar, Graz, Austria), using fluids prepared with 1 wt% alginate and NP2 (100 g/L and 200 g/L), either without CaCl$_2$ or with CaCl$_2$ (500 μL of 3 M CaCl$_2$ in 5 mL of 1% alginate, premixed with NP2). Fluids without NP2 were also analyzed for comparison. Strain amplitude sweeps were measured at a constant frequency of 6 rad/s, at 21 °C, and at strains ranging from 0.01 to 100%. All reported shear loss (G") and storage (G') moduli were measured in the region where they were independent of strain (i.e., in the linear region). Before addition of CaCl$_2$, the fluids were analyzed with a torque-controlled inner bob (radius = 13.33 mm, length = 40.01 mm) and a fixed outer measuring cup. Materials corsslinked with CaCl$_2$ were analyzed using parallel plate geometry (diameter = 50 mm), onto which sand paper was affixed to minimize slip.

2.6 Sorption Experiments

Sorption experiments were conducted at 21 °C using fluids prepared with 1 wt% alginate (5 mL) and NP2 (100 g/L and 200 g/L) and crosslinked with CaCl$_2$

(500 μL of 3 M CaCl$_2$ in 5 mL of 1% alginate, pre-mixed with NP2). Materials prepared without NP2 were also analyzed for comparison. Alginate-graphene materials were immersed in aqueous solution, obtained using 8.8 mL DI, 1.2 mL of 3 M CaCl$_2$, and 1.2 mL of 0.35 M Cr(VI), under no-flow conditions. The concentration of Cr(VI) was measured over time using a spectrophotometer (as described in Section 2.2) over time, up to approximately 250 min.

2.7 Material Restructuring Upon Exposure to an Electric Field

The effect of an applied electric field on the structure of alginate-graphene electrodes was investigated using the same materials described in Section 2.4. The materials were subjected to an electric field generated by a 10-V potential over different periods of time and up to 20 min, using a power source (Power Design Inc., 3650-S). In these experiments, the electrodes used were sectioned in two parts using a scalpel, to observe their internal structure.

3 Result and Discussions

The overall goal of this research is to provide a proof of concept that injectable electrodes can be used for the removal of Cr(VI) from water. This overall goal requires the development of materials with the following three properties: (1) good electrical conductivity, (2) ability to flow easily to the location of interest upon injection (i.e., polymeric fluids with low viscoelasticity), and (3) ability to form materials with good mechanical properties upon contact with a hardening agent (i.e., a crosslinker) after injection. We will first focus on each of these three aspects, before discussing the performance of the injectable electrodes in the removal of Cr(VI) from model aquifers (simulated with a cell filled with sand and saturated with water, as described in the materials and methods section).

3.1 Electrical Properties of Crosslinked Sodium Alginate Electrodes, With and Without Graphene Nanoplatelets

Voltammetric cycles were applied to investigate the electrical behavior of crosslinked alginate electrodes,

probing the effect of graphene nanoparticle type (NP1 vs. NP2) and graphene concentration. Sample voltammograms are shown in Figs. 2–3.

Voltage cycles showed that a very low current flowed through crosslinked sodium alginate without graphene nanoparticles. Specifically, when the voltage was varied between −0.5 V and +0.5 V, the maximum current was 25 μA (Fig. S1, supporting information). Voltage cycles also demonstrated that the amount of current flowing through sodium alginate depended on the nanoparticle type and concentration. Graphene was previously used to produce graphene–chitosan composite film, for the detection of 4-aminophenol (Yin et al., 2010). This study showed that the large specific area and good conductivity of graphene increased the electrochemical active sites and enhanced the electrochemical response of the material developed (Yin et al., 2010).

In our study, voltage cycles displayed a marked hysteresis with 200 g/L NP1 and 1 wt% sodium alginate, whereas with 200 g/L NP2, hysteresis was less marked. With 200 g/L NP1, when the voltage was ramped up to +5 V (forward scan) with steps of 0.5 V
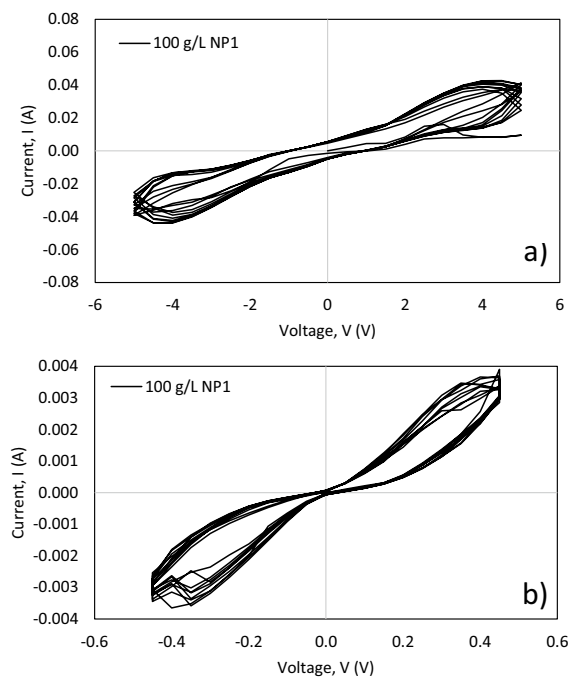

Fig. 2 Voltammogram measured using 100 g/L NP1, varying the voltage between either −5 and +5 V (**a**) or between −0.5 and +0.5 V (**b**)
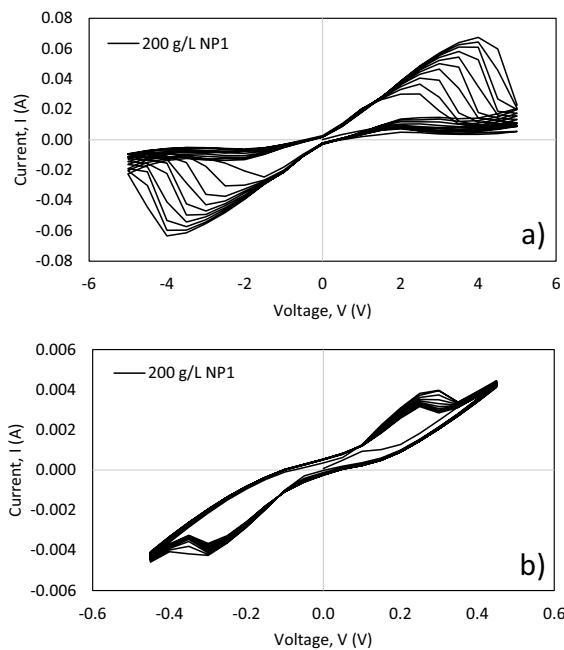
Fig. 3 Voltammogram measured using 200 g/L NP1, varying the voltage between either −5 and +5 V (**a**) or between −0.5 and +0.5 V (**b**)

Fig. 4 Voltammogram measured using 100 g/L (**a**) and 200 g/L (**b**) NP2, varying the voltage between −5 and +5 V

with a 2-s delay in between each step, the current increased monotonically up to approximately +4 V (to approximately 0.04 Å). Above this redox peak, the current decreased (Figs. 4–5). Also, when the voltage was ramped down from +5 to −5 V (backward scan), the slope of the I–V curve was approximately sixfold smaller compared to the forward scan. With 200 g/L NP1, hysteresis was also observed when the voltage was varied between +0.5 and −0.5 V. With 200 g/L NP2, a drop in current was also observed at approximately +4 V, but it was less significant than with NP1. Moreover, when the voltage was ramped down from +5 to −5 V (backward scan), the slope of the I–V curve was approximately threefold smaller compared to the forward scan (as opposed to the six-fold decrease observed with NP1). The differences between voltammetry curves measured with NP1 and NP2 are ascribed to differences in particle morphology, as will be further discussed later.

Hysteresis was less marked with 100 g/L than with 200 g/L of either NP1 or NP2 and 1 wt% sodium alginate. With 100 g/L graphene nanoparticles, the current increased monotonically with increasing voltage, as it was ramped up to +5 V
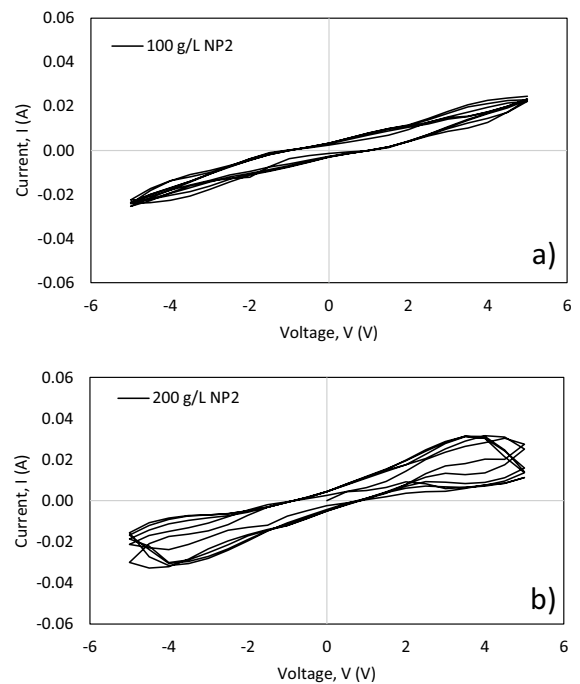
(forward scan): here, the current was approximately 40 mA with NP1 and 20 mA with NP2. Also, the slope of the I–V curve was in the forward, and backward scans were closer with 100 g/L than with 200 g/L graphene.

In cyclic voltammetry experiments, a significant concentration of the product is generated at the electrode proximity during the forward scan. In the backward scan, products return to their original oxidation state (Mabbott, 1983). Electrochemical reversibility depends on the electron transfer kinetics between the electrode and the material analyzed. Low barriers to electron transfer lead to electrochemical reversibility (Nernstian processes), whereas high barriers to electron transfer lead to electrochemical irreversibility and to hysteresis (Elgrishi et al., 2018). It is noted that the scan rate affects the reversibility of forward and backward cycles. At faster scan rates, slow electron kinetics lead to the appearance of redox peaks in I–V curves (Mabbott, 1983). Our results indicated that electron transfer was faster with 100 g/L than with 200 g/L NP1 graphene nanoparticles at the scan rates used, as shown by the marked redox peaks observed exclusively with 200 g/L NP1.
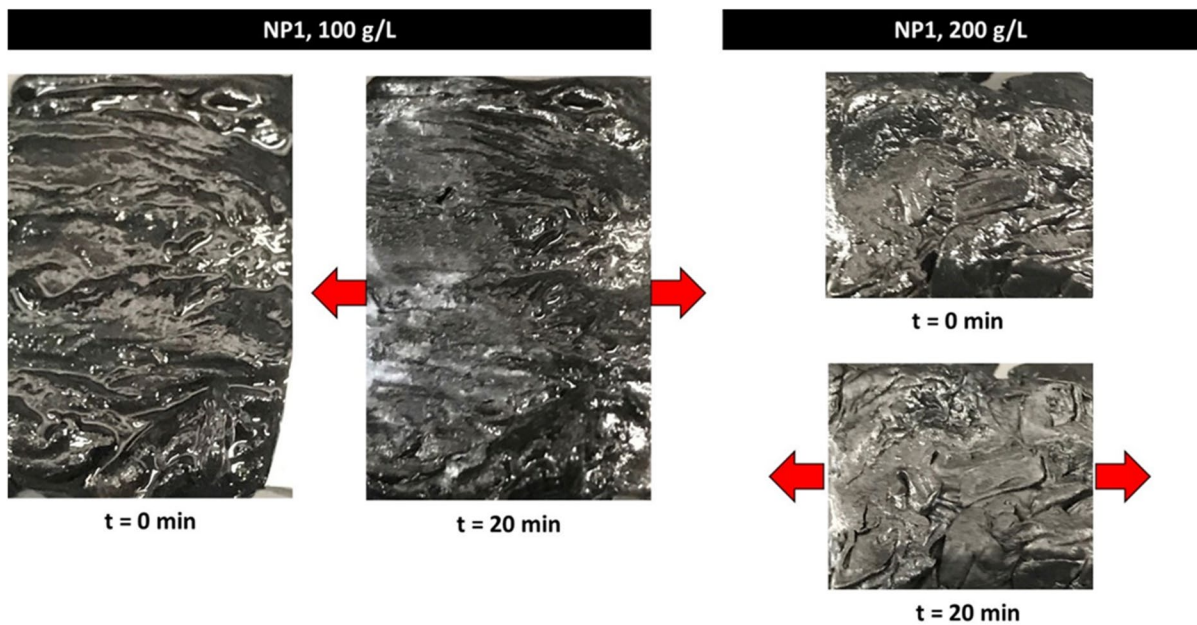
Fig. 5 Structuring of alginate-NP2 electrode upon exposure to an electric field generated by 10 V. Images were taken at different exposure times, ranging from time zero (when the experiment was started) to 10 min. The red arrows indicate the direction of the applied electric field

A previous study examined the electrical conductivity of lyophilized graphene oxide–chitosan (GO-CS) composite hydrogels (Sun et al., 2015). The authors found that conductivity increased with graphene oxide concentration, up to a benchmark value (Sun et al., 2015). The authors of that study hypothesized that graphene could promote electrolyte transport up to a benchmark concentration, because they favored the formation of pores through which electrolytes could migrate (Sun et al., 2015). Above a benchmark graphene oxide concentration, the conductivity of the composite materials decreased (Sun et al., 2015). Another study showed that electric fields can orient graphene oxide nanoplatelets in polymer matrices (e.g., in polyethersulfone matrices) (Besharat et al., 2020). This study reported that high loadings of graphene oxide could lead to agglomeration and disturb their alignment (Besharat et al., 2020). Another study used electric fields to orient clay in polydimethylsiloxane (Liu et al., 2018). This study reports that it was difficult to rotate clay particles with electric fields at high particle concentrations (Liu et al., 2018). Here, we hypothesize that at 200 g/L concentrations, graphene nanoparticles became jammed, and thus, particle reorientation was restricted. This

hypothesis would explain differences in the voltammetry experiments conducted at different nanoplatelet concentrations.

This hypothesis is also consistent with the observation that with 200 g/L NP1 and 1 wt% sodium alginate, the maximum current flow increased progressively in subsequent voltage cycles, and equilibrium could not be attained within five cycles. In contrast, with 100 g/L of either NP1 or NP2, I–V curves could reach equilibrium within 5 cycles. The increase in current flow in subsequent voltage cycles observed with 200 g/L of NP1 is known as "wake-up effect" (Walker et al., 2020). This behavior was previously reported, for instance, for the ferroelectric plastic crystal tetramethylammonium bromotrichloroferrate(III) (Walker et al., 2020). For this material, the wake-up effect was attributed to an increase in the fraction of ferroelectric domains switching in subsequent voltage cycles (Walker et al., 2020). Wake-up effects were also reported for polycrystalline AgNbO3-based antiferroelectric (AFE) materials and attributed to a phase transition from AFE to ferroelectric (FE) under low-field cycling (Lu et al., 2020). The wake-up effect observed for Si-doped HfO_2 was attributed to the annihilation of the disorder of the material analyzed

(Lee et al., 2018). The disorder of Si-doped HfO$_2$ was due to different factors, such as oxygen vacancies and interfacial defects (Lee et al., 2018).

Figures 5, 6 show the effects of an applied electric field (generated with a 10 V potential) on the structure of alginate-graphene electrodes. Qualitatively, electrode structure was heterogenous, with pores and channels present even before an electric field was applied. After 5-min exposure to an electric field, structuring was observed with electrodes prepared with 100 g/L of NP2. Structuring with 100 g/L NP1 required a longer time and was macroscopically visible after 20 min (although it was more subtle compared to when NP2 was used). Some structuring of electrodes prepared with 200 g/L NP2 occurred after 20-min exposure to the applied electric field, although macroscopic effects were significantly less marked than with 100 g/L NP2 (also, after 10-min, macroscopic differences in the material structure were not noticeable). Finally, macroscopic structuring of electrodes prepared with 200 g/L NP1 along the direction of the electric field could not be observed even after 20 min. These observations are consistent with cyclic voltammetry experiments, which showed that hysteresis and wake-up effects were most marked with 200 g/L NP1. Note that temperature and water evaporation were not controlled during the experiments conducted, and their effect cannot be discounted.

Differences between voltammetry curves and structuring of alginate-graphene electrodes containing NP1 and NP2 upon exposure to an electric field are ascribed to differences in the graphene size, as highlighted by SEM images (Figs. 7, 8) and as anticipated earlier in this section. SEM images showed that particles were polydisperse and that NP1 was on average larger than NP2. We speculate that hysteresis was more marked with NP1 than with NP2 because particles having larger sizes could not orient as easily as small particles upon exposure to an electric field. Furthermore, high concentrations of NP1 could have led to particle jamming, possibly increasing hysteresis. Previous studies demonstrated a correlation between particle size and the electrical behavior of materials. For instance, a study showed that the size of colloidal particles affects the Faraday charge and the redox potential of the particles (Heyrovsky & Jirkovsky, 1995). Another study
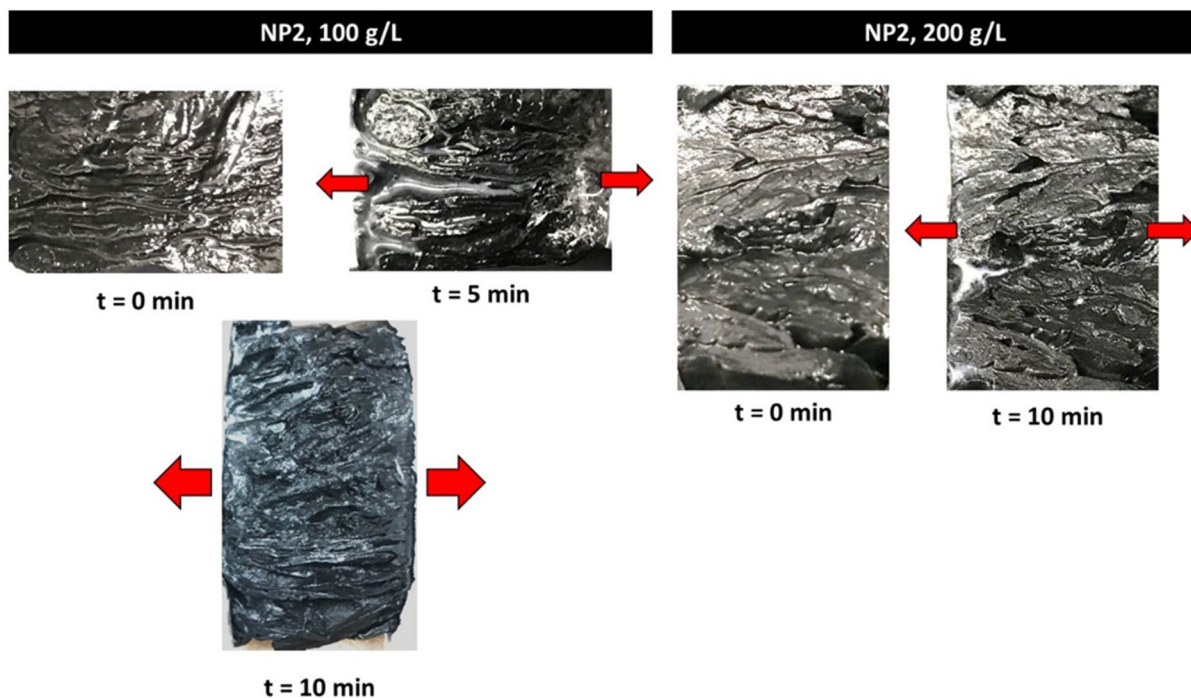

Fig. 6 Structuring of alginate-NP2 electrode upon exposure to an electric field generated by 10 V. Images were taken at different exposure times, ranging from time zero (when the experiment was started) to 10 min. The red arrows indicate the direction of the applied electric field

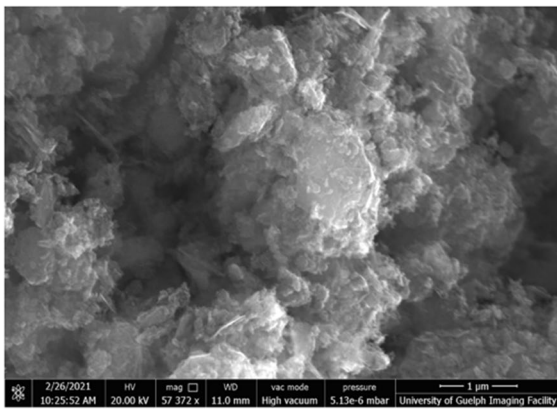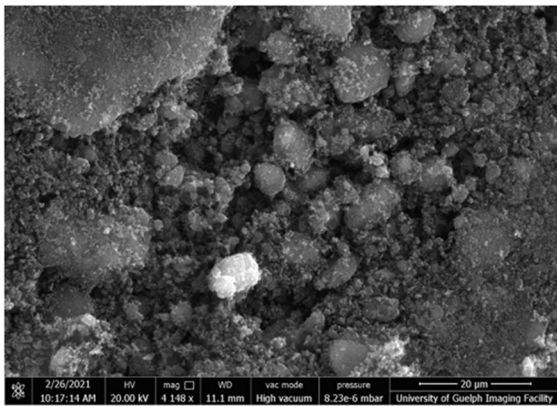**Fig. 7** Scanning electron microscopy images of NP1 at different magnifications
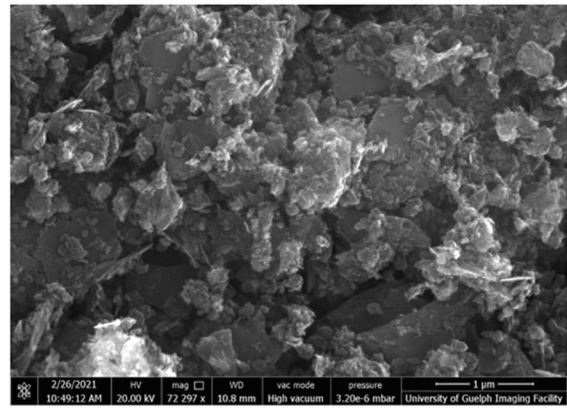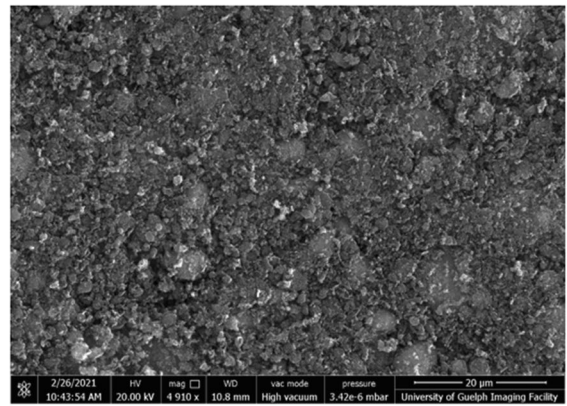

Fig. 8 Scanning electron microscopy images of NP2 captured at different magnifications. These images show that NP2 was smaller than NP1 (see Fig. 7 for comparison)

3.2 *Rheological Properties of Sodium Alginate Electrodes, With and Without Graphene Nanoplatelets, Before and After Crosslinking with CaCl$_2$*

As mentioned earlier, alginate-graphene nanoplatelets fluids should be injectable and flow easily to the location of interest upon injection. Also, they should form materials with good mechanical properties after injection, upon contact with a crosslinker (CaCl$_2$, in this study).

In addition to affecting conductivity, the presence and concentration of graphene nanoparticle concentration influenced the rheological behavior of sodium alginate-graphene nanoparticle solutions, both before and after crosslinking with Ca^{2+}, as determined using NP2. The viscoelastic moduli estimated in the linear region (where they were independent of strain) are reported in Table 1 and sample strain

investigated the effect of graphene size on the conductivity of graphene-based polymer composite films (Tarhini et al., 2021). In this study, composite films had the highest conductivity when the graphene flakes used had a larger average particle size (Tarhini et al., 2021).

In addition to the electrical properties of graphene-alginate electrode, the success of the proposed approach depends on the ease with which electrodes can be injected in the desired location and on their good mechanical properties after gelation. These characteristics are related to the rheology of the materials developed, as discussed in the next section (Section 3.2).

Table 1 Summary of the loss (G") and storage (G') moduli measured for sodium alginate, with and without NP2, before and after crosslinking with $CaCl_2$

System	G' (Pa)	G" (Pa)
1 wt% sodium alginate	0.14 ± 0.01	1.80 ± 0.01
1 wt% sodium alginate + 100 g/L NP2	16.90 ± 6.90	9.00 ± 0.22
1 wt% sodium alginate + 200 g/L NP2	109.20 ± 22.00	62.80 ± 6.40
1 wt% sodium alginate + $CaCl_2$	$47.10 \times 10^3 \pm 2.00 \times 10^3$	$11.70 \times 10^3 \pm 0.85 \times 10^3$
1 wt% sodium alginate + 100 g/L NP2 + $CaCl_2$	$1.01 \times 10^6 \pm 0.16 \times 10^6$	$1.70 \times 10^5 \pm 0.36 \times 10^5$

Values represent the average and standard deviation of $n = 3$ replicate measurements

sweeps are provided in the supporting information file (Figs. SI.2, SI.3).

Without $CaCl_2$ crosslinker or nanoparticles, 1 wt% alginate solutions were mainly viscous, with low loss and storage moduli (G' = 0.14 Pa and G" = 1.8 Pa). In contrast, 1 wt% alginate solutions with NP2 became mainly elastic, with higher storage and loss moduli compared to 1% alginate alone. This effect was most marked at the highest NP2 concentrations (G' ≈ 17 Pa, G" ≈ 9 Pa, and G'/G" ≈ 1.9 with 100 g/L NP2 and G' ≈ 109 Pa, G" ≈ 62 Pa, and G'/G" ≈ 1.8 with 200 g/L NP2). Flow is favored by low values of G' and G", whereas high G' and G" hinder transport (Lamont et al., 2019a; Marshall et al., 2020a; Pensini et al., 2018; Siwik et al., 2019). Therefore, using low nanoparticle concentrations (e.g., 100 g/L rather than 200 g/L) would be beneficial to facilitate the electrode injection, before crosslinking with Ca^{2+}.

After injecting alginate-graphene fluids, the injection of Ca^{2+} is required to crosslink sodium alginate, inducing gelation (Russo et al., 2007). After crosslinking with $CaCl_2$, without NP2, the storage modulus increased to G' ≈ 47.10×10^3 Pa, and the loss modulus increased to G" ≈ 11.70×10^3 Pa (G'/G" = 4). The increase of the storage and loss moduli was even more marked with 100 g/L NP2 (G' ≈ 11.01×10^6 Pa, G" ≈ 1.70×10^5 Pa and G'/G" ≈ 6). This result suggests attractive interactions between NP2 and alginate. A previous study reports that graphene oxide interacts with sodium alginate through hydrogen bonding, leading to the reinforcement of sodium alginate–based materials (Ionita et al., 2013). During the course of the electrokinetic experiments conducted (Section 2.3), alginate-graphene electrodes remained intact, because of their good mechanical properties. Moreover, the flow of elastic materials with G' > G" is inhibited (Marshall et al., 2020e),

ensuring that the injected electrodes remain in the desired position, in addition to being mechanically robust. This is required for their effective use in electrokinetic remediation. The next section (Section 3.3) demonstrates the effectiveness of alginate-graphene electrodes in removing Cr(VI), following their injection in a model aquifer.

3.3 Removal of Cr(VI) from Polluted Model Aquifers Using Alginate-Graphene Electrodes

The effectiveness of alginate-graphene electrodes was tested using either NP1 or NP2, at either 100 g/L or 200 g/L graphene concentrations. The percent Cr(VI) removal after different 10 min, 15 min, or 30 min treatments is reported in Table 2.

The data show that Cr(VI) removal was greater with 100 g/L NP1 than with NP2, using the same conditions (e.g., 15 min and 100 g/L of 1 wt% sodium alginate). This result is in agreement with the fact that the current measured was higher with 100 g/L NP1

Table 2 Removal of Cr(VI) using NP1

Treatment time (min)	% removal	Particle concentration (g/L)
NP1		
10	28.9 ± 7.6	100
15	45.8 ± 1.9	100
30	73.3 ± 5.2	100
NP2		
10	45.8 ± 2.2	100
15	59.1 ± 7.5	100
15	46.7 ± 3.6	200

Values represent the average and standard deviation of $n = 3$ replicate determinations

than with NP2 (Section 2.1). The data also show that increasing treatment time from 10 min to 15 min and to 30 min improved removal efficiency. In contrast, increasing the concentration of NP1 from 100 to 200 g/L decreased Cr(VI) removal efficiency. This result can be explained based on the voltammetry experiments (i.e., I–V curve measurements) discussed in Section 2.1. In particular, the electric current measured at the redox peak (at + 4 V) in the forward scan (i.e., increasing the voltage) with 200 g/L NP1 was higher than the current measured with 100 g/L platelets. However, with 200 g/L NP1, the current dropped at voltages above + 4 V, and the slope of the backward scan (i.e., decreasing the voltage) was significantly lower than the current measured in the forward scan.

Note that water samples after treatment were extracted from the entire sand cell, including from regions adjacent to the electrodes. The decrease in the concentration of Cr(VI) from the water extracted from the entire cell suggested that Cr(VI) was sorbed by the alginate-graphene nanoplatelets electrode, after migrating towards it.

Sorption experiments conducted under no-flow conditions confirmed this hypothesis, showing that alginate-NP2 materials sorbed Cr(VI) from water, as shown in Fig. 9. Sorption of Cr(VI) onto magnetic graphene (Hou et al., 2016) and onto expanded graphite (Hu et al., 2019) was previously reported. Graphene-containing aerogels were also used for the removal of Cr(VI) from water (Dong et al., 2018). Without graphene nanoplatelets, sodium alginate crosslinked with CaCl$_2$ could also sorb Cr(VI) from
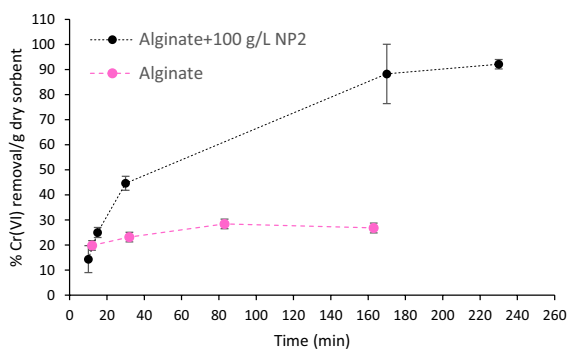

Fig. 9 Percent reduction of Cr(VI) concentration in DI water, starting from 0.35 mM Cr(VI). Values represent the average and standard deviation of $n = 2$ replicate determinations. The connecting lines are provided as a guide for the eye

water, albeit less effectively compared to when NP1 was added.

Sorbent electrodes have been previously proposed for the removal of cesium from wastewater (Chen et al., 2013). These sorbent electrodes enabled the removal of cesium without further treatment (Chen et al., 2013). In contrast, when non-sorbent electrodes are used, contaminants are either precipitated, pumped from the electrode proximity, or complexed with ion-exchange resins (Lu et al., 2012). In the case of treatment of groundwater contaminated with Cr(VI), sorbent electrodes would allow sequestering Cr(VI) from groundwater and reducing it at the cathode, following sorption.

4 Conclusions

This study used two types of graphene nanoparticles having different sizes (NP1 and NP2) and sodium alginate to produce unconventional electrodes. Our electrodes could be injected in the location of interest and solidified (gelled) using CaCl$_2$ (crosslinker). Shear rheology experiments demonstrated that CaCl$_2$ increased the viscoelastic moduli of the fluids and specifically the storage modulus (which exceeded the loss modulus after crosslinking). While gelation occurred even without graphene, graphene inclusion strengthened the material (increasing the storage moduli from approximately 47×10^3 Pa to 1.01×10^6 Pa with 100 g/L graphene). The formation of a gel after crosslinking would allow to form barriers around the treated areas, mitigating the risk of contaminant migration.

While both NP1 and NP2 increased the conductivity of crosslinked sodium alginate, NP1 yielded materials which enabled better Cr(VI) removal than NP2 upon applying an electric field. For materials containing 100 g/L NP1 in alginate, Cr(VI) concentrations were reduced by approximately 70% in 30 min in a model sandy aquifer (as demonstrated using a spectrophotometer). Differences in removal efficiency achieved with NP1 and NP2 are likely due to the different particle morphology. SEM images showed that NP1 were polydisperse and comprised larger aggregates and particles than NP2. Graphene concentration also affected removal efficiency, and the best results were achieved with 100 g/L NP1. In contrast, higher graphene concentrations (e.g., 200 g/L) reduced

Cr(VI) removal efficiency. Cyclic voltammetry experiments showed that hysteresis was more marked, and the equilibration time was longer when the graphene content in the alginate electrodes was increased from 100 g/L to 200 g/L.

Cr(VI) removal was achieved even without extracting (i.e., pumping) the pollutant from the electrode proximity, because alginate-graphene electrodes could sorb C(VI). Sorption experiments conducted under no-flow condition and without applying an electric field showed that graphene inclusion in crosslinked sodium alginate increased sorption from approximately 30 (without graphene) to 90% (with graphene) in 180 min. Our findings are a proof of concept of a novel remediation approach, which combines electrokinetic remediation with injectable barriers. Ongoing research in our lab focuses on applying this approach to the removal of other contaminants, including hydrocarbons and other heavy metals. Future research should also investigate the use of different types of conductive particles and polymer to produce injectable electrodes, with either improved performance or lower cost than the ones produced here. Finally, this research was conducted in a laboratory, and it requires validation on the field to fully assess its benefits and potential shortcomings.

References

Besharat F., Manteghian M., Gallone G., Lazzeri A., Electric field induced alignment of graphene oxide nanoplatelets in polyethersulfone matrix, *Nanotechnology*, 31 (2020) 155701.

Chen, R., Tanaka, H., Kawamoto, T., Asai, M., Fukushima, C., Na, H., Kurihara, M., Watanabe, M., Arisaka, M., & Nankawa, T. (2013). Selective removal of cesium ions from wastewater using copper hexacyanoferrate nanofilms in an electrochemical system. *Electrochimica Acta, 87*, 119–125.

Di Palma, L., Gueye, M. T., & Petrucci, E. (2015). Hexavalent chromium reduction in contaminated soil: A comparison between ferrous sulphate and nanoscale zero-valent iron. *Journal of Hazardous Materials, 281*, 70–76.

Dinesh, M., & Pittman, C. U. (2006). Activated carbons and low cost adsorbents for remediation of tri-and hexavalent chromium from water. *Journal of Hazardous Materials, 137*, 762–811.

Dong, S., Xia, L., Guo, T., Zhang, F., Cui, L., Su, X., Wang, D., Guo, W., & Sun, J. (2018). Controlled synthesis of flexible graphene aerogels macroscopic monolith as versatile agents for wastewater treatment. *Applied Surface Science, 445*, 30–38.

Elgrishi, N., Rountree, K. J., McCarthy, B. D., Rountree, E. S., Eisenhart, T. T., & Dempsey, J. L. (2018). A practical beginner's guide to cyclic voltammetry. *Journal of Chemical Education, 95*, 197–206.

Estepa, K. M. O., Lamont, K., Malicevic, S., Paschos, A., Colaruotolo, L., Corradini, M., Marangoni, A. G., Lim, L. T., & Pensini, E. (2020). Chitosan-based biogels: A potential approach to trap and bioremediate naphthalene. *Colloids and Surfaces A, 605*, 125374.

Guan, X., Sun, Y., Qin, H., Li, J., Lo, I. M. C., He, D., & Dong, H. (2015). The limitations of applying zerovalent iron technology in contaminants sequestration and the corresponding countermeasures: The development in zero-valent iron technology in the last two decades (1994–2014). *Water Research, 75*, 224–248.

Heyrovsky, M., & Jirkovsky, J. (1995). Polarography and voltammetry of ultrasmall colloids: Introduction to a new field. *Langmuir, 11*, 4288–4292.

Hou, T., Kong, L., Guo, X., Wu, Y., Wang, F., Wen, Y., & Yang, H. (2016). Magnetic ferrous-doped graphene for improving Cr (VI) removal. *Materials Research Express, 3*, 045006.

Hu, Z., Cai, L., Liang, J., Guo, X., Li, W., & Huang, Z. (2019). Green synthesis of expanded graphite/layered double hydroxides nanocomposites and their application in adsorption removal of Cr(VI) from aqueous solution. *Journal of Cleaner Production, 209*, 1216–1227.

Huang, W.-H., Dong, C.-D., Chen, C.-W., Surampalli, R. Y., & Kao, C.-M. (2017). Application of sulfate reduction mechanisms for the simultaneous bioremediation of toluene and copper contaminated groundwater. *International Biodeterioration & Biodegradation, 124*, 215–222.

Ionita, M., Pandele, M. A., & Iovu, H. (2013). Sodium alginate/graphene oxide composite films with enhanced thermal and mechanical properties. *Carbohydrate Polymers, 94*, 339–344.

Iyer, A., Pensini, E., & Singh, A. (2019). Removal of hexavalent chromium from water using hydrochar obtained with different types of feedstock. *Canadian Journal of Civil Engineering, 47*, 567–583.

Karn, B., Kuiken, T., & Otto, M. (2009). Nanotechnology and in situ remediation: A review of the benefits and potential risks. *Environmental Health Perspectives, 117*, 1813–1831.

Kim, S. O., Jeong, J. Y., Lee, W. C., Yun, S. T., & Jo, H. Y. (2020). Electrokinetic remediation of heavy metal-contaminated soils: Performance comparison between one- and two-dimensional electrode configurations. *Journal of Soils and Sediments*, 1–15.

Kim, W. S., Jeon, E. K., Jung, J. M., Jung, H. B., Ko, S. H., Seo, C. I., & Baek, K. (2014). Field application of electrokinetic remediation for multi-metal contaminated paddy soil using two-dimensional electrode configuration. *Environmental Science and Pollution Research, 21*, 4482–4491.

Lamont, K., Marangoni, A., & Pensini, E. (2019a). 'Emulsion locks' for the containment of hydrocarbons during surfactant flushing. *Journal of Environmental Sciences, 90*, 98–109.

Lamont, K., Pensini, E., & Marangoni, A. G. (2019b). Gelation on demand using switchable double emulsions: A potential strategy for the in situ immobilization of organic contaminants. *Journal of Colloid and Interface Science, 562*, 470–482.

Lee, T. Y., Lee, K., Lim, H. H., Song, M. S., Yang, S. M., Yoo, H. K., Suh, D. I., Zhu, Z., Yoon, A., MacDonald, M. R., & Lei, X. (2018). Ferroelectric polarization-switching dynamics and wake-up effect in Si-doped HfO2. *ACS Applied Materials & Interfaces, 11*, 3142–3149.

Liu, Z., Peng, P., Liu, Z., Fang, W., Zhou, Q., Liu, X., & Liu, J. (2018). Electric-field-induced out-of-plane alignment of clay in poly (dimethylsiloxane) with enhanced anisotropic thermal conductivity and mechanical properties. *Composites Science and Technology, 165*, 39–47.

Lu, P., Feng, Q., Meng, Q., & Yuan, T. (2012). Electrokinetic remediation of chromium-and cadmium-contaminated soil from abandoned industrial site. *Separation and Purification Technology, 98*, 216–220.

Lu, T., Tian, Y., Studer, A., Li, Q., Withers, R. L., Jin, L., Yu, D., Xu, Z., Wei, X., & Liu, Y. (2020). Structure-driven, ferroelectric wake-up effect for electrical fatigue relief. *Chemistry of Materials, 32*, 6456–6463.

Mabbott, G. A. (1983). An introduction to cyclic voltammetry. *Journal of Chemical Education, 60*, 697.

Manassero, M., Dominijanni, A., Foti, S., & Musso, G. (Eds.). (2013). *Coupled phenomena in environmental geotechnics*. CRC Press.

Marshall, T., Estepa, K., Corradini, M., Marangoni, A. G., Sleep, B., & Pensini, E. (2020b). Selective solvent filters for non-aqueous phase liquid separation from water. *Scientific Reports (accepted), 10*, 1–13.

Marshall, T., Gravelle, A., Laredo, T., Rodriguez-Uribe, A., Misra, M., Mohanti, A., Marangoni, A. G., Lim, L. T., & Pensini, E. (2020d). Zein-based materials: Effect of nanocarbon inclusion and potential applications. *Journal of Polymers and the Environment*, 1–10.

Marshall, T., Gravelle, A., Marangoni, A. G., Elsayed, A., & Pensini, E. (2020c). Zein for hydrocarbon remediation: Emulsifier, trapping agent, or both? *Colloids and Surfaces A, 589*, 124456.

Marshall, T., Marangoni, A. G., Corradini, M. G., Rodriguez-Uribe, A., Misra, M., Mohanty, A. K., Rodriguez, B. M., & Pensini, E. (2020a). Path-dependent rheology of carbon particle-hydroxyethylcellulose fluids. *Colloids and Surfaces A, 612*, 126000.

Marshall, T., Marangoni, A. G., Lim, L. T., Tchoukov, P., & Pensini, E. (2020e). Oxidizing emulsifiers: Gelators for water in hydrocarbon reactive emulsions. *Journal of Environmental Chemical Engineering, 9*, 104998.

Mulligan, C. N., Yong, R. N., & Gibbs, B. F. (2001). Remediation technologies for metal-contaminated soils and groundwater: An evaluation. *Engineering Geology, 60*, 193–207.

Němeček, J., Pokorný, P., Lacinová, L., Černík, M., Masopustová, Z., Lhotský, O., Filipová, A., & Cajthaml, T. (2015). Combined abiotic and biotic in-situ reduction of hexavalent chromium in groundwater using nZVI and whey: A remedial pilot test. *Journal of Hazardous Materials, 300*, 670–679.

Němeček, J., Pokorný, P., Lhotský, O., Knytl, V., Najmanová, P., Steinová, J., Černík, M., Filipová, A., Filip, J., & Cajthaml, T. (2016). Combined nano-biotechnology for in-situ remediation of mixed contamination of groundwater by hexavalent chromium and chlorinated solvents. *Science of the Total Environment, 563*, 822–834.

Pensini, E., Elsayed, A., Rodriguez, B. M., Marangoni, A. G., Singh, A., Sleep, B., Hayward, G., Lamont, K., & Collier, C. M. (2018). In situ trapping and treating of hexavalent chromium using scleroglucan-based fluids: A proof of concept. *Colloids and Surfaces A, 559*, 192–200.

Pokharel, P., Xiao, D., Erogbogbo, F., & Keles, O. (2019). A hierarchical approach for creating electrically conductive network structure in polyurethane nanocomposites using a hybrid of graphene nanoplatelets, carbon black and multi-walled carbon nanotubes. *Composites Part b: Engineering, 161*, 169–182.

Reddy, K. R., & Chinthamreddy, S. (2004). Enhanced electrokinetic remediation of heavy metals in glacial till soils using different electrolyte solutions. *Journal of Environmental Engineering, 130*, 442–455.

Reddy, K. R., Maturi, K., & Cameselle, C. (2009). Sequential electrokinetic remediation of mixed contaminants in low permeability soils. *Journal of Environmental Engineering, 135*, 989–998.

Russo, R., Malinconico, M., & Santagata, G. (2007). Effect of cross-linking with calcium ions on the physical properties of alginate films. *Biomacromolecules, 8*, 3193–3197.

Sawada, A., Mori, K. I., Tanaka, S., Fukushima, M., & Tatsumi, K. (2004). Removal of Cr (VI) from contaminated soil by electrokinetic remediation. *Waste Management, 24*, 483–490.

Siwik, A., Pensini, E., Elsayed, A., Rodriguez, B. M., Marangoni, A. G., & Collier, C. M. (2019). Natural guar, xanthan and carboxymethyl-cellulose-based fluids: Potential use to trap and treat hexavalent chromium in the subsurface. *Journal of Environmental Chemical Engineering, 7*, 102807.

Su, H., Fang, Z., Tsang, P. E., Fang, J., & Zhao, D. (2016). Stabilisation of nanoscale zero-valent iron with biochar for enhanced transport and in-situ remediation of hexavalent chromium in soil. *Environmental Pollution, 214*, 94–100.

Sun, G., Li, B., Ran, J., Shen, X., & Tong, H. (2015). Three-dimensional hierarchical porous carbon/graphene composites derived from graphene oxide-chitosan hydrogels for high performance supercapacitors. *Electrochimica Acta, 171*, 13–22.

Tarhini, A., Tehrani-Bagha, A., Kazan, M., & Grady, B. (2021). The effect of graphene flake size on the properties of graphene-based polymer composite films. *Journal of Applied Polymer Science, 138*, 49821.

Thatoi, H., Das, S., Mishra, J., Rath, B. P., & Das, N. (2014). Bacterial chromate reductase, a potential enzyme for bioremediation of hexavalent chromium: A review. *Journal of Environmental Management, 146*, 383–399.

Virkutyte, J., Sillanpää, M., & Latostenmaa, P. (2002). Electrokinetic soil remediation — Critical overview. *Science of the Total Environment, 289*, 97–121.

Walker, J., Miranti, R., Skjærvø, S. L., Rojac, T., Grande, T., & Einarsrud, M. A. (2020). Super-coercive electric field hysteresis in ferroelectric plastic crystal tetramethylammonium bromotrichloroferrate (III). *Journal of Materials Chemistry C, 8*, 3206–3216.

Wang, L., Huang, L., Xia, H., Li, H., Li, X., & Liu, X. (2019). Application of a multi-electrode system with polyaniline auxiliary electrodes for electrokinetic remediation of chromium-contaminated soil. *Separation and Purification Technology, 224*, 106–112.

Yan, Y., Xue, F., Muhammad, F., Yu, L., Xu, F., Jiao, B., Shiau, Y., & Li, D. (2018). Application of iron-loaded activated carbon electrodes for electrokinetic remediation of chromium-contaminated soil in a three-dimensional electrode system. *Scientific Reports, 8*, 1–11.

Yin, H., Ma, Q., Zhou, Y., Ai, S., & Zhu, L. (2010). Electrochemical behavior and voltammetric determination of 4-aminophenol based on graphene–chitosan composite film modified glassy carbon electrode. *Electrochimica Acta, 55*, 7102–7108.

Zhou, H., Xu, J., Lv, S., Liu, Z., & Liu, W. (2020). Removal of cadmium in contaminated kaolin by new-style electrokinetic remediation using array electrodes coupled with permeable reactive barrier. *Separation and Purification Technology, 239*, 116544.